

Identification of candidate millisecond pulsars from *Fermi* LAT observations

Xue-Jie Dai^{1,2}, Zhong-Xiang Wang¹, Jithesh Vadakkumthani¹ and Yi Xing¹

¹ Shanghai Astronomical Observatory, Chinese Academy of Sciences, Shanghai 200030, China; wangzx@shao.ac.cn

² University of Chinese Academy of Sciences, Beijing 100049, China

Received 2015 December 28; accepted 2016 February 9

Abstract We report our detailed data analysis of 39 γ -ray sources selected from the 992 unassociated sources in the third *Fermi* Large Area Telescope Third Source Catalog. The selection criteria, which were set for finding candidate millisecond pulsars (MSPs), are non-variables with curved spectra and $>5^\circ$ Galactic latitudes. From our analysis, 24 sources were found to be point-like sources not contaminated by background or nearby unknown sources. Three of them, J1544.6–1125, J1625.1–0021 and J1653.6–0158, have been previously studied, indicating that they are likely MSPs. The spectra of J0318.1+0252 and J2053.9+2922 do not have properties similar to known γ -ray MSPs, and we thus suggest that they are not MSPs. Analysis of archival X-ray data for most of the 24 sources was also conducted. Four sources were found with X-ray objects in their error circles, and 16 with no detection. The ratios between the γ -ray fluxes and X-ray fluxes or flux upper limits are generally lower than those of known γ -ray MSPs, suggesting that if the γ -ray sources are MSPs, none of the X-ray objects are their counterparts. Deep X-ray or radio observations of these sources are needed in order to identify their MSP nature.

Key words: stars: pulsars — stars: binaries — gamma rays: stars

1 INTRODUCTION

The *Fermi* Gamma-Ray Space Telescope (*Fermi*), with its great capabilities, has revolutionized our view of the high-energy, γ -ray sky. Thus far, the detection of 3033 sources has been reported in the *Fermi* Large Area Telescope (LAT) Third Source Catalog (hereafter called the third source catalog) (Acero et al. 2015), which used 4 yr of science data (years 2008–2012) from *Fermi* LAT all-sky monitoring observations. Among the sources, most of them are Active Galactic Nuclei (AGNs; Ackermann et al. 2015), but in our Galaxy a prominent class is pulsars. According to the second *Fermi* LAT catalog of γ -ray pulsars and a public list of LAT-detected γ -ray pulsars¹, 161 pulsars have been detected with γ -ray pulsations and more than 20 new millisecond pulsars (MSPs) have been discovered due to *Fermi* LAT detection of them. These results have not only established pulsars as the main γ -ray sources in the Galaxy, which has long been suspected from surveys of the sky with previous Gamma-Ray telescopes, for example the *Compton Gamma-Ray Observatory* (Thompson 2008), but also helped to significantly improve our studies of the pulsar population, in particular MSPs.

MSPs are $\sim 10^9$ yr old, fast spinning neutron stars, which have evolved from low-mass X-ray binaries by accreting from companions and thus gaining sufficient an-

gular momentum (Alpar et al. 1982; Radhakrishnan & Srinivasan 1982). Due to their relatively high efficiency η of converting spin-down energy \dot{E} to γ -ray emission (because $\eta \propto 1/\dot{E}$; e.g., Abdo et al. 2013) and isotropic distribution in the sky, *Fermi* all-sky monitoring is a powerful tool for finding new candidate MSPs, although note that it is extremely difficult to identify them from blind searches of pulsation signals in the *Fermi* LAT data (e.g., Pletsch et al. 2012). One important result due to *Fermi* is the discovery of a significant number of eclipsing MSP binaries, namely black widows (Fruchter et al. 1988) and redbacks (Roberts 2013). As pointed out by Roberts (2013), the number of such systems has increased by 6-times to ~ 20 . Moreover three redbacks, PSR J1023+0038 (Archibald et al. 2009), J1824–2452I (in the globular cluster M28; Papitto et al. 2013) and XSS J12270–4859 (Bassa et al. 2014), are also known as transitional pulsar binaries, which can switch between the states of having an accretion disk and being disk-free. How to explain the presence of these systems and their formation processes is an interesting question (Chen et al. 2013; Benvenuto et al. 2014).

Since approximately one third of *Fermi* LAT sources have not been identified or found in association with any known objects (Acero et al. 2015) and pulsars are prominent γ -ray sources, it is conceivable that a significant number of pulsars are among these un-associated sources. We have carried out a systematic study of them, aiming to identify MSPs among them. In this paper, we report target

¹ <https://confluence.slac.stanford.edu/display/GLAMCOG/Public+List+of+LAT-Detected+Gamma-Ray+Pulsars>

selection from the third source catalog of candidate MSPs (101 sources are found; see Sect. 1.1) and results from data analysis of 39 selected targets. In Section 1.1, the detailed selection process is described, which is based on the properties of pulsars derived from *Fermi* studies. We present our analysis of the LAT data and archival X-ray data for the targets in Section 2. The results and discussion are given in Section 3.

1.1 Candidate Target Selection

From *Fermi* LAT observations, it has been learned that emission from pulsars is stable. This feature greatly helps in distinguishing them from more dominant AGN sources. The latter are strong variables at multi-wavelengths including γ -ray (e.g., Williamson et al. 2014). In addition, the *Fermi* γ -ray spectra of pulsars generally have the form of a power law with an exponential cutoff (PLE), with cut-off energies at several GeV (Abdo et al. 2013), i.e., some degree of curvature in their spectra is one feature of their emission. For comparison, AGNs generally have ‘straight’ power law (PL) spectra (e.g., Ackermann et al. 2015).

We thus selected candidate MSP targets from high Galactic sources in the third source catalog, since MSPs generally have an isotropic distribution (Abdo et al. 2013). A Galactic latitude of $> 5^\circ$ was used, which helped avoid the crowded Galactic plane. Then requiring that the sources have variability indices less than 72.44 (99% confidence for a source not being a variable) and curvature significance greater than 3σ (Acero et al. 2015), 101 sources were selected from the third source catalog. Their positions in Galactic coordinates are shown in Figure 1. As can be seen, nearly 40% of them are located within Galactic longitudes of $\pm 30^\circ$, implying there is a high concentration towards the direction of the Galactic center. Such a distribution suggests that they are likely associated with the Milky Way.

2 DATA ANALYSIS

2.1 *Fermi* LAT Data

LAT, one of the two main instruments onboard *Fermi*, is an imaging γ -ray telescope conducting an all-sky survey in the energy range from 20 MeV to 300 GeV. It was designed such that γ -ray events can be distinguished from background events through measuring the direction, energy and arrival time of each γ -ray photon (Atwood et al. 2009). In the analysis of this paper, the data for each target we used are selected from the *Fermi* Pass 7 Reprocessed database within 15° of the target’s position. The time period spans from 2008 August 4 15:43:39 to 2015 January 22 16:08:17 (UTC; nearly 6.5 yr), and the energy range is from 200 MeV to 300 GeV to avoid the relatively large uncertainties of the instrument response function of the LAT in the low energy range. Following the recommendations of the LAT team, we selected events with zenith angles less

than 100° to exclude possible contamination from Earth’s limb.

2.1.1 Maximum likelihood analysis

For each of our targets, we performed a standard binned maximum likelihood analysis (Mattox et al. 1996) on the data using the LAT science tools software package v9r33p0. Based on the third source catalog, all sources within 25° centered at the position of each target were included to make the source model. The spectral parameters of these sources are provided in the catalog. The spectral normalization parameters of the sources within 5° of each target, which were considered if they were detected with $> 5\sigma$ significance, were set free. All the other parameters were fixed at their catalog values. Considering the Galactic and extragalactic diffuse emission, we added the model `gll_iem_v05_rev1.fits` and the spectrum file `iso_source_v05.txt` to the source model. The normalization parameters of the diffuse emission were left free as well.

We obtained the Test Statistic (TS) map of a $2^\circ \times 2^\circ$ region centered at the position of each target. Defined as $TS = -2 \log(L_0/L_1)$, where L_0 and L_1 respectively are the maximum likelihood values for a model without and with an additional source at a specified location (Abdo et al. 2010b), the square root of a TS value is approximately equal to the detection significance for a given source. By examining the TS map of each target, we identified ‘isolated’ point-like sources among them, which we defined not to be mixed with other unknown sources or located in a region with strong, extended emission. We considered them to be ‘clean’ targets. We then ran `gtfindsrc` in the LAT software package to determine accurate positions for these clean targets. Among the initially selected 39 sources, there are 27 such clean sources. They are listed in Tables 1 and 2. The best-fit positions we obtained are consistent with those provided in the third source catalog within 2σ error circles.

The other 12 sources are not clean point sources, as indicated by the TS maps we obtained.

In Figure 2, two such examples are shown. They were found to be mixed with other unknown sources and/or located in a region with strong background. Further analysis of the groups of sources or the extended emission, which will help determine their true emission features, requires a large amount of computing time. Therefore these 12 sources were excluded from our target list. To be complete, their spectral parameters provided in the third source catalog are given here in Table 3. The spectra of J0004.2+6757 and J1827.7+1141 were fitted with a PL model, and the other 10 sources have spectra modeled with a LogParabola model,

$$\frac{dN}{dE} = N_0 \left(\frac{E}{E_b} \right)^{-\alpha - \beta \log(E/E_b)}, \quad (1)$$

where N_0 , α and β are flux density, photon index and the curvature, respectively. The energy E_b was set

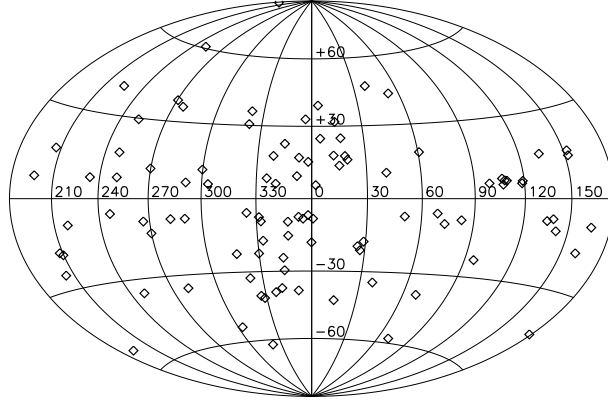


Fig. 1 Galactic positions of the selected 101 sources from the third source catalog. Nearly 40% of them are located within Galactic longitudes of $\pm 30^\circ$.

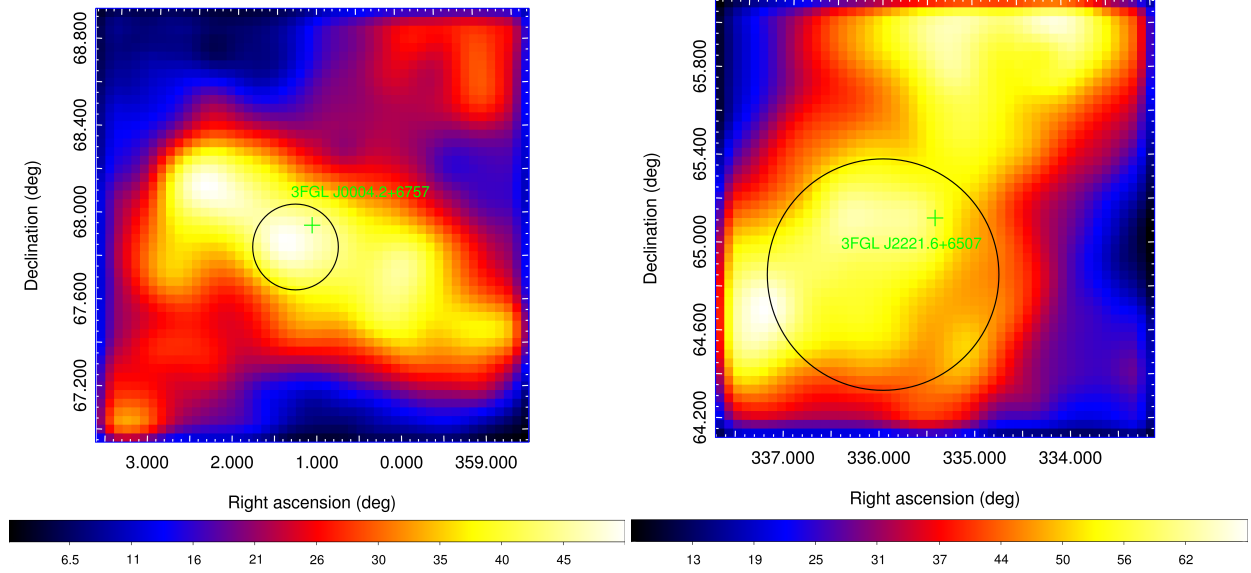


Fig. 2 Examples of the targets that were found to be mixed with other unknown sources from the TS maps. The green plus signs indicate the position from the third source catalog, and the solid circles indicate the 2σ positional error circles we estimated for the targets.

such that errors on differential fluxes were minimal, and “Signif_Curve” is the curvature significance estimated from likelihood values for a PL model or a LogParabola model.

2.1.2 Spectral analysis

We extracted the γ -ray spectra for the clean point-like sources by performing two separate fits at their best-fit positions. First, we modeled each source with a simple PL

$$\frac{dN}{dE} = N_0 \left(\frac{E}{E_0} \right)^{-\Gamma}, \quad (2)$$

where N_0 is the normalization, Γ is the photon index and we set $E_0 = 1$ GeV. We evenly divided energy logarithmically from 0.1 to 300 GeV into 15 energy bands for the spectral analysis, and kept the photon index fixed to the value obtained from running *glike* at the best-fit position. For our results, only spectral data points with $TS > 4$ were kept. As mentioned above, pulsars generally have exponentially cutoff power-law spectra. We secondly repeated the analysis using a PLE

$$\frac{dN}{dE} = N_0 \left(\frac{E}{E_0} \right)^{-\Gamma} \exp\left(-\frac{E}{E_c}\right), \quad (3)$$

Table 1 Spectral Results for Candidate Millisecond Pulsars

Source name	Spectral model	Flux/ 10^{-9} (photons $\text{cm}^{-2} \text{s}^{-1}$)	Γ	E_c (GeV)	TS	Signif_Curve (σ)	Comments
J0212.1+5320	PowerLaw	14.5 ± 0.9	2.17 ± 0.04		848	9.11	
	PLSuperExpCutoff	10.8 ± 0.9	1.3 ± 0.1	2.6 ± 0.5	924		
J0238.0+5237	PowerLaw	12 ± 1	2.38 ± 0.06		319	5.14	
	PLSuperExpCutoff	10 ± 1	1.8 ± 0.2	4 ± 1	341		
J0312.1–0921	PowerLaw	6.0 ± 0.8	2.26 ± 0.08		190	5.13	c-subhalo
	PLSuperExpCutoff	4.0 ± 0.8	1.2 ± 0.3	2.0 ± 0.6	211		
J0318.1+0252	PowerLaw	5.8 ± 0.7	2.19 ± 0.07		191	6.54	c-subhalo
	PLSuperExpCutoff	2.6 ± 0.4	0.00 ± 0.03	1.0 ± 0.3	231		non-MSP
J0336.1+7500	PowerLaw	9.5 ± 0.8	2.24 ± 0.05		389	6.67	
	PLSuperExpCutoff	7.1 ± 0.8	1.5 ± 0.2	3.0 ± 0.8	431		
J0545.6+6019	PowerLaw	5.6 ± 0.7	2.03 ± 0.06		279	5.15	
	PLSuperExpCutoff	4.0 ± 0.6	1.4 ± 0.2	7 ± 2	303		
J0758.6–1451	PowerLaw	7.5 ± 0.9	2.32 ± 0.07		212	4.91	
	PLSuperExpCutoff	5.2 ± 0.9	1.4 ± 0.3	2.3 ± 0.8	234		
J0935.2+0903	PowerLaw	6.2 ± 0.8	2.5 ± 0.1		135	3.32	
	PLSuperExpCutoff	5.0 ± 0.9	1.7 ± 0.4	1.8 ± 0.8	145		
J0953.7–1510	PowerLaw	5.4 ± 0.6	2.13 ± 0.07		227	6.73	c-subhalo
	PLSuperExpCutoff	2.1 ± 0.6	0.6 ± 0.4	1.5 ± 0.4	269		
J1120.6+0713	PowerLaw	6.0 ± 0.7	2.20 ± 0.07		249	6.49	AGN (?)
	PLSuperExpCutoff	4.0 ± 0.6	1.0 ± 0.3	1.7 ± 0.4	292		
J1225.9+2953	PowerLaw	7.0 ± 0.7	2.11 ± 0.06		436	6.59	c-subhalo
	PLSuperExpCutoff	4.7 ± 0.7	1.3 ± 0.2	3.3 ± 0.8	469		
J1544.6–1125	PowerLaw	12 ± 1	2.54 ± 0.07		262	3.47	c-MSP
	PLSuperExpCutoff	11 ± 1	2.1 ± 0.2	3 ± 2	27		
J1625.1–0021	PowerLaw	16.5 ± 0.8	2.09 ± 0.03		1261	13.16	c-MSP
	PLSuperExpCutoff	10.5 ± 0.8	0.8 ± 0.2	1.9 ± 0.2	1433		
J1627.8+3217	PowerLaw	3.6 ± 0.5	2.15 ± 0.08		158	4.55	
	PLSuperExpCutoff	2.4 ± 0.5	1.2 ± 0.3	3 ± 1	178		
J1653.6–0158	PowerLaw	31 ± 1	2.32 ± 0.03		1686	9.43	c-MSP
	PLSuperExpCutoff	27 ± 1	1.75 ± 0.08	3.3 ± 0.5	1747		
J1730.6–0357	PowerLaw	7 ± 1	2.17 ± 0.08		124	4.49	
	PLSuperExpCutoff	4 ± 1	1.1 ± 0.4	3 ± 1	143		
J1950.2+1215	PowerLaw	15 ± 2	2.9 ± 0.1		149	3.13	
	PLSuperExpCutoff	13 ± 2	2.2 ± 0.3	2 ± 1	151		
J2026.8+2813	PowerLaw	10 ± 1	2.57 ± 0.09		87	4.91	
	PLSuperExpCutoff	7 ± 2	0.9 ± 0.6	0.9 ± 0.3	111		
J2053.9+2922	PowerLaw	1.3 ± 0.3	1.59 ± 0.09		114	5.52	non-MSP
	PLSuperExpCutoff	0.5 ± 0.1	0.2 ± 0.5	8 ± 3	146		
J2103.7–1113	PowerLaw	6.2 ± 0.7	2.18 ± 0.07		239	4.31	c-subhalo
	PLSuperExpCutoff	4.4 ± 0.8	1.4 ± 0.3	3 ± 1	255		
J2117.6+3725	PowerLaw	15 ± 1	2.57 ± 0.06		314	4.16	
	PLSuperExpCutoff	14 ± 1	2.0 ± 0.2	2.5 ± 0.9	327		
J2212.5+0703	PowerLaw	7.1 ± 0.8	2.27 ± 0.07		209	5.29	c-subhalo
	PLSuperExpCutoff	5.0 ± 0.8	1.4 ± 0.3	2.5 ± 0.8	236		
J2233.1+6542	PowerLaw	21 ± 2	2.69 ± 0.07		240	4.60	
	PLSuperExpCutoff	19 ± 2	1.9 ± 0.3	1.6 ± 0.6	252		
J2250.6+3308	PowerLaw	5.0 ± 0.8	2.5 ± 0.1		81	3.97	
	PLSuperExpCutoff	4.0 ± 0.8	1.2 ± 0.5	1.1 ± 0.5	96		

where E_c is the cutoff energy. By comparing results from the two spectral models, the curvature significance Signif_Curve was obtained, which was estimated from $\text{Signif_Curve} = \sqrt{2 \log(L_{\text{PLE}}/L_{\text{PL}})}$, where L_{PLE} and L_{PL} are the maximum likelihood values modeled with PLE and PL, respectively.

From this analysis, we found that for three sources, whose spectral results are given in Table 2, a PLE model is not significantly better than a PL one. Among them,

J1601.9+2306 had a TS value from a PL model larger than that from a PLE. Their spectra are shown in Figure 4. We therefore excluded these three sources from our target list.

2.1.3 Variability analysis

As a further check, we performed timing analysis of the LAT data for the 24 remaining sources. The time period from 2008 August 4 23:59:59 to 2014 December 31

Table 2 Sources without Sufficient Curvature Significance

Source name	Spectral model	Flux/ 10^{-9} (photon $\text{cm}^{-2} \text{s}^{-1}$)	Γ	E_c (GeV)	TS	Signif_Curve (σ)
J1543.5–0244	PowerLaw	8 ± 1	2.7 ± 0.1		103	2.22
	PLSuperExpCutoff	7 ± 1	2.2 ± 0.3	4 ± 3	107	
J1601.9+2306	PowerLaw	4.4 ± 0.8	2.3 ± 0.1		107	3.55
	PLSuperExpCutoff	1 ± 2	0.0 ± 0.1	1.2 ± 0.6	102	
J1722.7–0415	PowerLaw	11 ± 1	2.49 ± 0.09		121	0.68
	PLSuperExpCutoff	11 ± 2	2.4 ± 0.2	24 ± 34	121	

Table 3 Sources without Clean Background

Source name	Spectral model	Flux density/ 10^{-12} (photon $\text{cm}^{-2} \text{MeV}^{-1} \text{s}^{-1}$)	Γ	E_0 (MeV)	Signif_Avg (σ)	Signif_Curve (σ)	
J0004.2+6757	PowerLaw	0.6 ± 0.1	2.5	1328.36	6.01	3.91	
J1827.7+1141	PowerLaw	0.18 ± 0.03	2.1	1960.79	6.49	3.81	
Source name	Spectral model	Flux density/ 10^{-12} (photon $\text{cm}^{-2} \text{MeV}^{-1} \text{s}^{-1}$)	α	β	E_b (MeV)	Signif_Avg (σ)	Signif_Curve (σ)
J0008.5+6853	LogParabola	4.3 ± 0.5	2.4	0.9	820.26	8.45	6.49
J0345.3+3236	LogParabola	6.8 ± 0.9	2.4	1.0	641.45	7.68	5.00
J0431.7+3503	LogParabola	2.1 ± 0.3	2.6	0.3	941.06	7.85	4.02
J0539.2–0536	LogParabola	11 ± 1	2.5	1.0	556.20	7.35	5.10
J1729.9–0859	LogParabola	19 ± 2	2.6	1.0	445.58	7.18	5.40
J2125.8+5832	LogParabola	4.4 ± 0.6	2.4	1.0	774.12	7.47	4.01
J2206.5+6451	LogParabola	4.5 ± 0.5	2.8	0.7	803.49	8.60	6.03
J2221.6+6507	LogParabola	6.1 ± 0.8	2.6	0.9	678.66	7.45	4.80
J2221.7+6318	LogParabola	7.0 ± 0.8	2.5	1.0	739.95	8.42	6.65
J2310.1–0557	LogParabola	0.49 ± 0.08	1.8	0.8	1490.34	8.97	5.35

Table 4 Properties of X-ray Sources Detected in the Error Circles of Four Candidate MSPs

Source name	R.A. (h: m: s)	Dec. ($^{\circ}$: $'$: $''$)	$N_H/10^{20}$ (cm^{-2})	Γ	$F_{0.3-10}^{\text{unabs}}$	χ^2/DoF	G_{100}	$G_{100}/F_{0.3-10}^{\text{unabs}}$
(1)	(2)	(3)	(4)	(5)	(6)	(7)	(8)	(9)
J0212.1(S)	02:12:10.46	+53:21:37.62	17.4	$1.04^{+0.47}_{-0.46}$	$1.85^{+0.78}_{-0.51}$	3.1/4(C)	16.6	9.0
J0212.1(C)	02:12:10.50	+53:21:38.94	17.4	$1.35^{+0.05}_{-0.06}$	$1.77^{+0.07}_{-0.06}$	115/107	16.6	9.4
J1120.6(S)	11:20:42.54	+07:13:12.74	4.24	$0.74^{+0.96}_{-1.07}$	$0.73^{+1.40}_{-0.44}$	2.4/2(C)	6.2	8.5
J1627.8(S)	16:27:42.85	+32:20:58.56	1.87	$3.07^{+1.56}_{-1.08}$	$0.43^{+0.71}_{-0.19}$	5.6/3(C)	3.1	7.2
J2103.7(C)	21:03:49.99	–11:13:40.62	4.70	$1.71^{+0.22}_{-0.20}$	$0.16^{+0.021}_{-0.020}$	24/13	6.9	43
J2103.7(C)	21:03:52.31	–11:11:32.66	4.70	$1.77^{+0.25}_{-0.24}$	$0.10^{+0.021}_{-0.017}$	17/21	6.9	69

Notes: (1) Source name, where *S* or *C* indicate the *Swift* or *Chandra* observation used in the analysis, respectively, and the observation IDs (exposure time) in the sequence listed in the table are 00041276001 (3.3 ks), 14814 (30 ks), 0003164100 (4.3 ks), 00041418001 (3.5 ks) and 12381 (30 ks); (2)–(3) Right Ascension (R.A.) and Declination (Dec.) of each X-ray source, epoch J2000.0; (4) Absorption column density; (5) PL index; (6) Unabsorbed flux in the 0.3–10 keV band (in units of $10^{-12} \text{ erg cm}^{-2} \text{ s}^{-1}$); (7) The χ^2/DoF value for the model, where the Cash statistic is indicated by C; (8) *Fermi* LAT flux in the energy range of 0.1–100 GeV (in units of $10^{-12} \text{ erg cm}^{-2} \text{ s}^{-1}$); (9) Flux ratio between G_{100} and $F_{0.3-10}^{\text{unabs}}$.

23:59:57 (UTC) was divided into 30-day intervals. We adopted the PL model leaving the photon index fixed at the value obtained in Section 2.1.2 and conducted maximum likelihood analysis in each time bin at the best-fit position of each source. The lightcurves and TS curves were thus extracted. No significant flux variations were seen from the

30-day interval lightcurves, which are consistent with the results in the third source catalog for them.

2.2 X-ray Data Analysis

We searched for possible X-ray counterparts to the 24 γ -ray sources. Among them, J1544.6–1125 has been studied

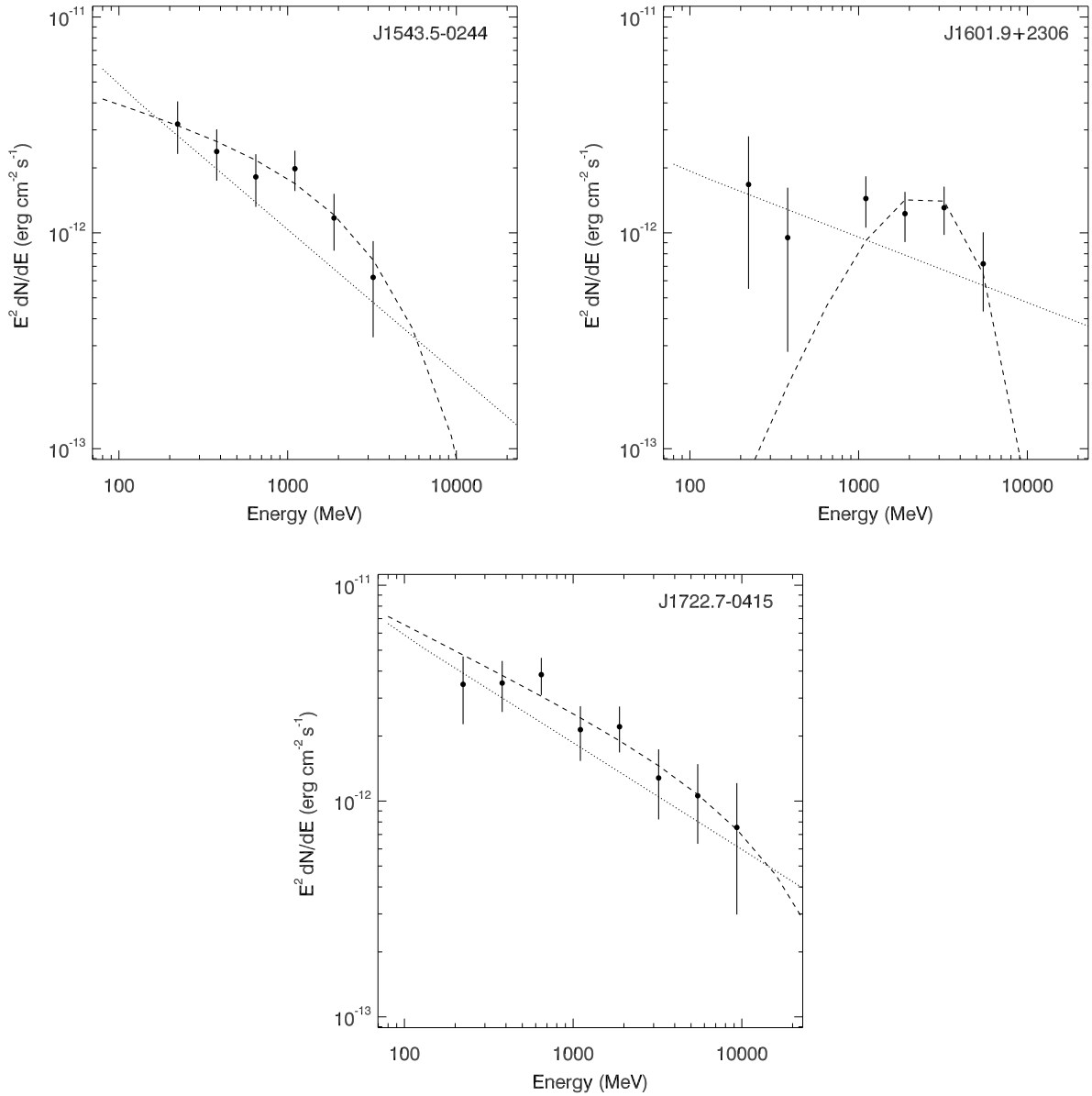


Fig. 3 γ -ray spectra of J1543.5–0244 (*top left*), J1601.9+2306 (*top right*) and J1722.7–0415 (*bottom*). The dotted and dashed curves are the best-fit PL and PLE models respectively.

at multiple wavelengths (including X-rays) and suggested to be a transitional MSP due to its similar emission properties (Bogdanov & Halpern 2015; Bogdanov 2015), and J1625.1–0021 and J1653.6–0158 have been studied at X-ray energies and searched for potential optical/infrared counterparts (Kong et al. 2014; Hui et al. 2015). No analysis of their archival data was conducted. For each of the rest of the targets, its 2σ positional uncertainty region covered by any archival X-ray imaging data from the *XMM-Newton*, *Chandra* or *Swift* telescopes was searched and analyzed. We found that four γ -ray sources had X-ray sources in their uncertainty regions, and 16 were covered by short *Swift* observations but showed no detection of any X-ray sources.

For the detections, the *Chandra* data were reprocessed using the script *chandra_repro* in the *Chandra* Interactive Analysis Observation software (CIAO 4.6). We used the source detection tool in CIAO (CELLDETECT) for source detection. A circular region with a $10''$ radius centered at a source was used to extract the source’s photons, and a nearby source-free region with the same size was taken as the background. The source and background spectra were obtained with the CIAO tool PSEXTRACT. We used χ^2 statistics in the spectral fitting.

Among the available *Swift* data for each target, we selected the dataset with the longest exposure time when there were multiple sets of data. The *Swift* XRT data were processed using the XRTDAS software included in the

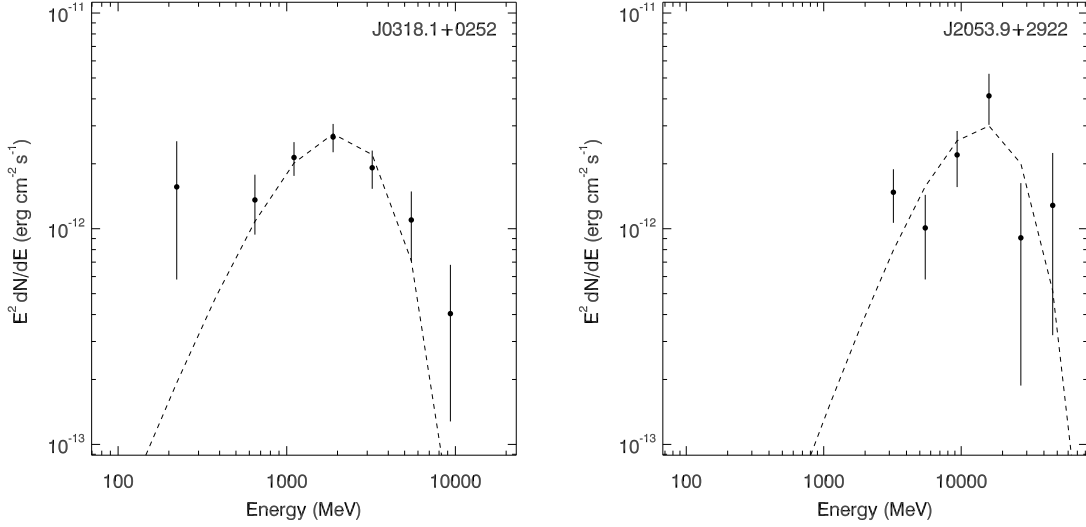


Fig. 4 γ -ray spectra of J0318.1+0252 (*left panel*) and J2053.9+2922 (*right panel*), with the dashed curves being the best-fit PLE models.

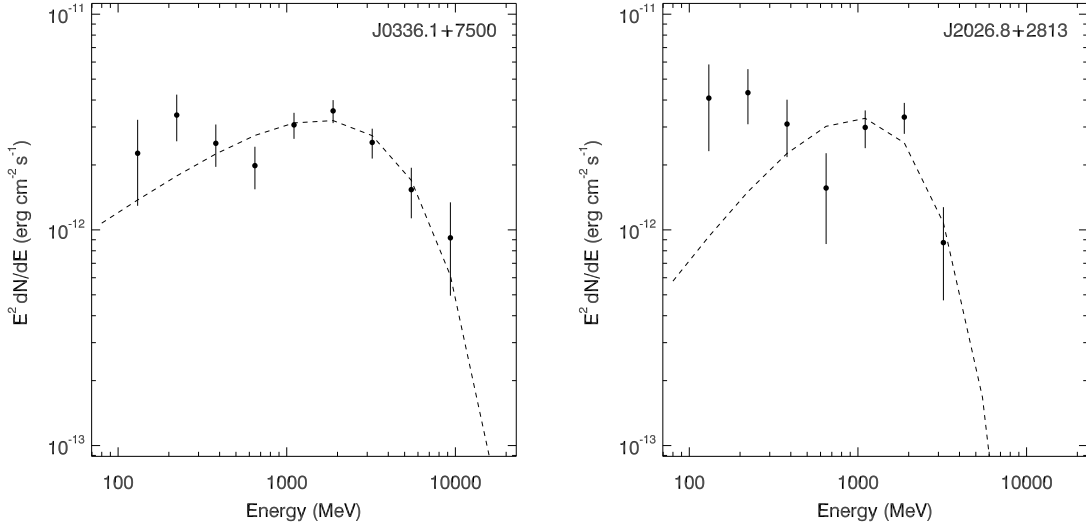


Fig. 5 γ -ray spectra of J0336.1+7500 (*left panel*) and J2026.8+2813 (*right panel*). The dashed curves indicate the best-fit PLE models, which do not describe the spectral data points well, as the spectra probably have two components.

HEASOFT package (version 6.13) distributed by the High Energy Astrophysics Science Archive Research Center (HEASARC). For each observation, calibrated and cleaned PC-mode event files were produced with the XRTPIPELINE task. We used the XIMAGE detection algorithm DETECT to locate X-ray point sources in the XRT images. The positions of the detected sources were then refined by using the task XRTCENTROID that is part of the XRTDAS package. We extracted photons from a circular region with a $47''$ radius around a source and from a nearby source-free region with the same size as the background. We adopted the Cash C statistic (Cash 1979) for spectral modeling due to the few net counts.

In the spectral fitting, due to the limited photon counts for most of our sources, only an absorbed PL was used as the model, where we fixed the absorption column density to the Galactic value (Dickey & Lockman 1990) in the direction of each source. The obtained spectral parameters are given in Table 4. The PL photon indices range from $\sim 1 - 2$ for these sources and suggest that the X-ray emission is mostly non-thermal in nature. However, for the source J1627.8+3217, the PL model results in a large photon index, $\Gamma \sim 3.1$, which probably suggests a thermal scenario instead for this source. We thus also examined its spectrum with an absorbed blackbody model, where the absorption was fixed at the Galactic value. We found a tem-

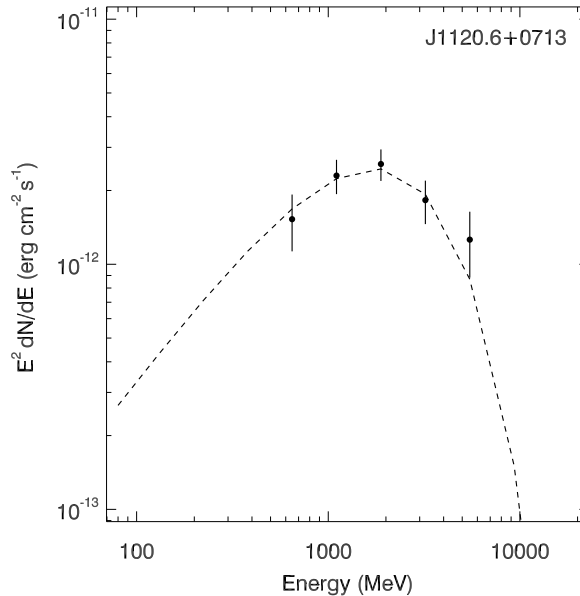


Fig. 6 γ -ray spectrum of J1120.6+0713, with the dashed curve indicating the best-fit PLE model.

perature of $kT = 0.19_{-0.06}^{+0.11}$ keV with $C = 5.9$ for 3 degrees of freedom (DoF). This model provides a more reasonable description of the data. For the source J2103.7-1113, two X-ray sources within the 2σ *Fermi* error circle were detected, and both were well described by an absorbed PL model.

For the non-detections, which resulted from short *Swift* observations, we estimated 3σ upper limits on fluxes from the count rates using the webPIMMS². An absorbed PL spectrum with a photon index of 1.7 was assumed, and the absorption column density to a source was fixed at the Galactic value in the direction of the source (Dickey & Lockman 1990). The flux upper limits for the *Fermi* sources are given in Table 5.

3 RESULTS AND DISCUSSION

Having analyzed the LAT data of 39 un-associated sources selected from the third source catalog, we found 27 clean point-like sources among them. Further requiring curvature significance in a spectrum, 24 sources were selected. Their spectral results are provided in Table 1. Among the 24 sources, J1544.6–1125 has already been well studied at multiple wavelengths, particularly X-rays, and suggested to be a transitional MSP (Bogdanov & Halpern 2015; Bogdanov 2015). The sources J1625.1–0021 and J1653.6–0158 have been studied as well and are listed as promising candidate MSPs (Hui et al. 2015). Moreover, an orbital period of 75 min was found for the second source from optical imaging, indicating its likely nature of being an MSP binary (Kong et al. 2014). These studies support our target selection and further data analysis selection.

Examining the obtained spectra, we note that since MSPs generally have γ -ray spectra with Γ and E_c in the ranges of 0.4–2.0 and 1.1–5.4 GeV respectively (see Abdo et al. 2013 for details), the sources J0318.1+0252 and J2053.9+2922 have parameters of $\Gamma = 0.00 \pm 0.03$ and 0.2 ± 0.5 , and $E_c = 1.0 \pm 0.3$ GeV and 8 ± 3 GeV, respectively. The values, particularly for the first source, are not within the ranges defined from known γ -ray MSPs. Their spectra are shown in Figure 4. As can be seen, the spectra have a fast drop in the low 0.1–1 GeV energy range, not containing significant emission, thus making Γ close to zero. Given that they exhibit such a spectral property, they are likely not MSPs. In addition, the sources J0336.1+7500 and J2026.8+2813 appear to possibly have two components in their spectra, which are shown in Figure 5. We examined their TS maps and they are consistent with being point sources. Their TS maps at low (0.1–1.0 GeV) and high (1.0–300 GeV) energy ranges were also calculated, but no evidence was found from the TS maps for the cases such as the presence of an additional source in the region. These two sources are of interest for further investigation.

We note that source J1120.6+0713 was listed as an AGN in the first catalog of AGNs detected by *Fermi* LAT (associated with CRATES J1120+0704; Abdo et al. 2010a), but it was not in the third source catalog (Ackermann et al. 2015). The spectrum we obtained, which is shown in Figure 6, is well described by a PLE model. In addition, six sources in Table 1 were listed as promising dark matter subhalo candidates in Bertoni et al. (2015). The double identification is due to their selection criteria of non-variables with Galactic latitudes $> 20^\circ$ (similar to ours) and curved spectra calculated from dark matter annihilation models. In any case, the likely MSPs

² <http://heasarc.gsfc.nasa.gov/cgi-bin/Tools/w3pimms/w3pimms.pl>

Table 5 X-ray Flux Upper Limits for the Candidate MSPs

Source name	ObsID	Exp (s)	$N_{\text{H}}/10^{20}$ (cm^{-2})	$F_{0.3-10}^{\text{upper}}/10^{-13}$ ($\text{erg cm}^{-2} \text{s}^{-1}$)	$G_{100}/10^{-12}$ ($\text{erg cm}^{-2} \text{s}^{-1}$)	$G_{100}/F_{0.3-10}^{\text{upper}}$
(1)	(2)	(3)	(4)	(5)	(6)	(7)
J0238.0	00047142003	3363	26.3	< 2.8	13	> 46
J0312.1	00047144004	3738	6.23	< 1.2	5.9	> 49
J0318.1	00084649005	1817	8.77	< 1.9	5.1	> 27
J0336.1	00047146002	1672	14.3	< 4.3	11	> 26
J0545.6	00084664005	2066	14.7	< 3.6	8.3	> 23
J0758.6	00041341002	2569	11.6	< 1.6	7.3	> 46
J0935.2	00084964006	668	3.53	< 4.5	5.7	> 13
J0953.7	00031656001	3517	5.29	< 1.3	5.6	> 43
J1225.9	00041382001	4005	1.79	< 0.76	8.4	> 110
J1730.6	00084792002	1672	14.1	< 3.1	7.2	> 23
J1950.2	00085096001	802	1.76	< 8.1	52	> 64
J2026.8	00085106001	2462	32.9	< 2.2	7.9	> 36
J2117.6	00041492001	3716	17.0	< 1.2	15	> 130
J2212.5	00047320001	2497	6.47	< 3.2	7.3	> 23
J2233.1	00084887001	2670	59.1	< 2.6	20	> 77
J2250.6	00085140002	1952	7.87	< 2.4	4.5	> 19

Notes: (1) Source name; (2) ID of the *Swift* observation used for the analysis; (3) Exposure time in seconds for each observation; (4) Absorption column density; (5) The 3σ upper limit on flux in the 0.3–10 keV band (a PL with 1.7 photon index was assumed); (6) *Fermi* LAT flux in the energy range of 0.1–100 GeV; (7) Lower limits on the flux ratio between G_{100} and $F_{0.3-10}^{\text{upper}}$.

J1544.6–1125 and J1625.1–0021 (see above) are also in their list, indicating the possibly high chance of identifying an MSP as a candidate dark matter subhalo. Information about the possible nature of these sources is provided in Table 1.

Finally for the candidate MSPs in Table 1 that were covered by X-ray observations, we calculated their G_{100} flux, which is defined as the total γ -ray flux in the energy range of 0.1–100 GeV (Abdo et al. 2013). The γ -ray-to-X-ray flux ratios (for the cases of having X-ray sources in the source field) or lower limits on the flux ratios (for the cases of non-detection) were then estimated. The values are given in Tables 4 and 5. For most of the known γ -ray MSPs, the ratios are in a range of 100–1000 (see table 16 in Abdo et al. 2013). This property suggests that none of the X-ray sources listed in Table 4 are their counterparts. In addition, if we consider that the sources in Table 5 are MSPs, their lower flux-ratio limits of $> 20 - 100$ suggest that the X-ray observations are not sufficiently deep for detecting any X-ray counterparts. Further X-ray observations of them are needed in order to identify their MSP nature by finding X-ray counterparts.

Acknowledgements This research made use of the High Performance Computing Resource in the Core Facility for Advanced Research Computing at Shanghai Astronomical Observatory. This research was supported by the National Natural Science Foundation of China (11373055) and the Strategic Priority Research Program “The Emergence of Cosmological Structures” of the Chinese Academy

of Sciences (Grant No. XDB09000000). Z.W. acknowledges the support by the CAS/SAFEA International Partnership Program for Creative Research Teams; J.V. by the Chinese Academy of Sciences President’s International Fellowship Initiative (CAS PIFI, Grant No. 2015PM059); and Y.X. by the Shanghai Natural Science Foundation for Youth (13ZR1464400) and the National Natural Science Foundation of China for Youth (11403075).

References

- Abdo, A. A., Ackermann, M., Ajello, M., et al. 2010a, *ApJ*, 714, 927
- Abdo, A. A., Ackermann, M., Ajello, M., et al. 2010b, *ApJS*, 188, 405
- Abdo, A. A., Ajello, M., Allafort, A., et al. 2013, *ApJS*, 208, 17
- Acero, F., Ackermann, M., Ajello, M., et al. 2015, *ApJS*, 218, 23
- Ackermann, M., Ajello, M., Atwood, W. B., et al. 2015, *ApJ*, 810, 14
- Alpar, M. A., Cheng, A. F., Ruderman, M. A., & Shaham, J. 1982, *Nature*, 300, 728
- Archibald, A. M., Stairs, I. H., Ransom, S. M., et al. 2009, *Science*, 324, 1411
- Atwood, W. B., Abdo, A. A., Ackermann, M., et al. 2009, *ApJ*, 697, 1071
- Bassa, C. G., Patruno, A., Hessels, J. W. T., et al. 2014, *MNRAS*, 441, 1825

- Benvenuto, O. G., De Vito, M. A., & Horvath, J. E. 2014, *ApJ*, 786, L7
- Bertoni, B., Hooper, D., & Linden, T. 2015, *J. Cosmol. Astropart. Phys.*, 12, 035
- Bogdanov, S. 2015, arXiv:1508.05844
- Bogdanov, S., & Halpern, J. P. 2015, *ApJ*, 803, L27
- Cash, W. 1979, *ApJ*, 228, 939
- Chen, H.-L., Chen, X., Tauris, T. M., & Han, Z. 2013, *ApJ*, 775, 27
- Dickey, J. M., & Lockman, F. J. 1990, *ARA&A*, 28, 215
- Fruchter, A. S., Stinebring, D. R., & Taylor, J. H. 1988, *Nature*, 333, 237
- Hui, C. Y., Park, S. M., Hu, C. P., et al. 2015, *ApJ*, 809, 68
- Kong, A. K. H., Jin, R., Yen, T.-C., et al. 2014, *ApJ*, 794, L22
- Mattox, J. R., Bertsch, D. L., Chiang, J., et al. 1996, *ApJ*, 461, 396
- Papitto, A., Ferrigno, C., Bozzo, E., et al. 2013, *Nature*, 501, 517
- Pletsch, H. J., Guillemot, L., Fehrmann, H., et al. 2012, *Science*, 338, 1314
- Radhakrishnan, V., & Srinivasan, G. 1982, *Current Science*, 51, 1096
- Roberts, M. S. E. 2013, in *IAU Symposium*, 291, *Neutron Stars and Pulsars: Challenges and Opportunities after 80 years*, ed. J. van Leeuwen, 127
- Thompson, D. J. 2008, *Reports on Progress in Physics*, 71, 116901
- Williamson, K. E., Jorstad, S. G., Marscher, A. P., et al. 2014, *ApJ*, 789, 135